ELSEVIER

The effect of fillers on the fresh and hardened properties of 3D printed geopolymer lattices

Paolo Scanferla [a], Alberto Conte [b], Agusti Sin [b], Giorgia Franchin [a,*], Paolo Colombo [a,c]

[a] *Department of Industrial Engineering, University of Padova, 35131, Padova, Italy*
[b] *ITT Motion Technologies, Barge, CN, Italy*
[c] *Department of Material Science and Engineering, The Pennsylvania State University, 16802, University Park, PA, USA*

ABSTRACT

This work analyzed the effect of particle fillers on the rheology of geopolymer-based inks and on the micro-structure and mechanical properties of lattices fabricated by Direct Ink Writing and subjected to different curing and firing temperatures. Adding particle fillers effectively improved the printability of the pure geopolymer ink; ground geopolymer filler was the most effective. In particular, it increased the yield strength and storage modulus, speeded up the recovery after extrusion and expanded the working window.

The mechanical response of the lattices did not increase with the addition of fillers nor with increased curing temperature and time; curing at 80 °C for 1 day was the best compromise between strength and time. The filler influenced the mechanical properties of lattices as a function of the firing temperature. Samples without fillers had a maximum strength of 34 ± 3 MPa after firing at 300 °C, whereas those containing sand were damaged by the treatment; samples containing ground geopolymer were the most stable up to 1000 °C.

1. Introduction

It is well known that geopolymers are inorganic materials that are obtained by the reaction between a solid alumino-silicate source and an alkaline solution, typically containing an alkali silicate and an alkali hydroxide. The alumino-silicate component can be metakaolin or it can be derived by waste, such as fly ash. Typical features of geopolymers include setting at room to low (e.g. 40–80 °C) temperature, fast setting times (of the order of minutes to tens of minutes), good compression strength (up to a few tens of MPa), hydraulicity of the reaction product (provided by the continuous, amorphous 3D network developed), and intrinsic mesoporosity [1]. Because of these features, they have been proposed as substitutes for Portland cement (OPC) in mortar or concrete formulations [2–4], but also as absorbents for a wide range of pollutants in water, either in the form of powders, pellets or foams [5].

However, because of their composition, they have also been used for the production of ceramic materials, such as Nepheline [6], Leucite [7], Pollucite [8], Mullite [9,10], silicon nitride [11] and silicon carbide [12], obtained either by firing at moderate to high temperatures, taking advantage also of carbothermal reduction reactions occurring when a carbon source is added to the formulation, or by substituting alkaline ions by ion-exchange followed by a thermal treatment. The *in situ*

ceramization of geopolymers has also been exploited for the production of passive fire-resistant components [13].

Investigations on Additive Manufacturing of geopolymers have so far been carried out using two techniques: Binder jetting (BJ) [14,15] and Direct Ink Writing (DIW) [16–20], with the latter being preferred because it provides components with higher strength and the possibility of using wide-diameter nozzles for large-scale manufacturing of building components, using mortar or concrete formulations. In this context, several protocols were developed in order to understand and characterize the rheological properties of geopolymer mixtures. The simplest approach would be to exploit qualitative, on-site tests for conventional concrete, such as the flow table test, the portable vane test and the uni-axial unconfined compression test. With this approach, a concrete mixture with 20% alkali-activated materials (AAMs) substitution on the cement paste was characterized and its workability (i.e., flowability of the mixture) and buildability (i.e. shape retention after extrusion) was found suitable for an extrusion-based 3D printing process [21]. However, fundamental differences have been detected in the viscoelasticity be-tween AAMs and conventional cement pastes with a thorough rheolog-ical characterization. Performing a small amplitude oscillatory shear (SAOS) test, Alnahhal et al. [22] monitored the early stage structural build-up due to the transformation of solid aluminates and silicates into

---

an aluminosilicate gel. The high viscosity of alkaline solutions in AAMs resulted in reduced colloidal interactions between particles and therefore in lower yield stress; a weak elastic network was observed and attributed to delayed flocculation at the early stages, whereas the solid-like state was achieved over time as a result of stiffening [22]. Muthukrisnan et al. [23] set up a characterization protocol specific for extrusion-based 3D printing of geopolymer concrete, representing in each test one stage of printing operation (pumping, extrusion and building). A complete rheological characterization requires to assess the flow behavior (flow sweep), the elastic-to-viscous transition (large amplitude oscillatory sweep, LAOS), the structural recovery and the setting of the geopolymer mixtures.

In this paper, we expand on our previously published work [16], by exploring the use of particulate additives to further enhance the control of the rheology of the geopolymer ink. Our focus is not on the fabrication of building components, but of highly porous functional parts; therefore, curing and firing at different temperatures was also explored and the influence of fillers on the microstructure and mechanical properties upon the different heat treatments was assessed. The rheology characterization protocol developed in our previous work [16] was replicated for the newly developed mixtures to allow for a comparison between inks with and without fillers.

When using small nozzles (e.g. with a diameter <1 mm), high resolution cellular architectures can be fabricated with a significant degree of accuracy, and a wide range of different morphologies can be obtained [16,17]. Applications of such structures, when processed only at room temperature, can be found in pollutant removal [24] or heterogeneous catalysis [25]. Heat treated scaffolds could be used as monolithic ceramic supports for catalysts operating at intermediate to high temperatures [26, 27], providing considerable advantages with respect to honeycombs or foams because of their non stochastic architecture, and the possibility of achieving, through topological optimization [28], a much better control and improvements in pressure drop, mechanical strength, contact time and tortuosity of flow paths.

2. Materials and methods

2.1. Samples preparation

Na-based geopolymer inks were prepared by mixing metakaolin (Argical 1200S, Imerys S.A., Italy) as an aluminosilicate source, and an alkaline solution of sodium silicate (SS2942, Ingessil S.r.l., Italy), sodium hydroxide (NaOH, Sigma–Aldrich) and distilled water. The alkaline solution had a molar ratio of $SiO_2/Na_2O = 1.4$ and solids content of 38.5 wt %. The molar ratios of the geopolymer were: $SiO_2/Al_2O_3 = 3.8$, $Na_2O/Al_2O_3 = 1$ and $H_2O/Al_2O_3 = 13$. As a rheological additive, 5 wt% of polyethylene glycol with an average molecular weight of 1000 g/mol (PEG 1000, Sigma-Aldrich, Italy) was added to the ink. The ink preparation follows the same procedure described elsewhere [16] and this ink was labelled GP.

For some formulations, 20 vol% of filler in powder form was added to the inks; the filler was either siliceous sand (Sabbia Po Fine, Bacchi S.p.A, Italy) or geopolymer powder. Inks with sand and ground geopolymer as fillers were labelled GPS and GPP, respectively. The composition of the sand is reported in the Supplementary Information. The geopolymer powder had the same composition of the fresh geopolymer component of the ink, and it was produced in the same way (without PEG addition). It was then cast in a closed mold, cured at 80 °C for 24 h and finally crushed. The fillers were sieved below 300 μm and their granulometric distribution was evaluated by sieve analysis; the data are reported in the Supplementary Information. The sand had D_{10} ~130 μm, D_{50} ~225 μm and D_{90} ~285 μm; the ground geopolymer had D_{10} ~50 μm, D_{50} ~100 μm and D_{90} ~205 μm.

The filler was added to the ink before the metakaolin addition, and stirred at 1000 rpm for 10 min. In this case, the final metakaolin addition required mixing at higher energy (rotation speed up to 1800 rpm) and an

ice bath was placed around the ink to decrease its temperature and limit water evaporation.

The ink was stored at about 4 °C for 30 min and then loaded in the DIW device (Delta WASP 2040 Turbo, WASP, Italy), which is equipped with a pressurized vessel and an infinite screw for paste extrusion. The printing process was carried out at room temperature and in air, extruding the ink through the tip of a conical nozzle with a diameter of 840 μm (Nordson Italia S.p.a., Italy) at about 10 mm/s. The printed geometry was a $20.0 \times 20.0 \times 7.2$ mm^3 log-pile structure with a 0–90° stacking, layer height of 600 μm and gaps set at 1600 μm (from the centers of two filaments). Each lattice took about 5 min to be produced. After printing, the samples were placed in a sealed box and subjected to different curing treatments in ambient air: room temperature, 40 °C and 80 °C for either 1 day or 7 days.

Different firing temperatures were also investigated, to determine the most effective post-treatment of the lattices and their high temperature behavior. Samples were cured at 80 °C for 1 day and then treated at 300 °C, 500 °C, 700 °C and 1000 °C in static atmospheric air with a 1 °C/min heating ramp and a 1 h dwelling step, followed by cooling in the furnace.

2.2. Rheological characterization of the ink

A rotational rheometer (Kinexus Pro+, Malvern, Italy) equipped with a 25 mm diameter sanded plate–plate geometry was used, with a set temperature of 20 °C and a gap of 1 mm. Several tests were performed on the inks comprising sand and geopolymer powder as fillers, and results were compared with those previously published for a pure geopolymer ink of the same composition [16]:

- Steady rate sweep: shear rate increasing from 1 to 5 1/s.
- Dynamic strain sweep: frequency set to 1 Hz while deformation increases from 0.001 to 100%.
- Moduli recovery in two steps:
1. Constant strain of 70% (to overcome the initial yield stress and break the geopolymer network) with 1 Hz frequency for 60 s;
2. Constant strain of 0.1% with 1 Hz frequency for 120 s.
- Working time: constant deformation of 0.01% with a frequency of 0.1 Hz over 1 h.

2.3. Physical and mechanical characterization

The microstructure of the printed lattices was investigated using an optical stereomicroscope (STEMI 2000-C, Carl Zeiss AG, Italy) and an environmental scanning electron microscope (ESEM, Quanta 200, FEI, Italy).

X-ray diffraction analysis (Bruker AXS D8 Advance, Bruker Corp., Italy) was performed on powdered samples after each thermal treatment. The crystalline phases were identified by Match! Software (Crystal Impact GbR) with ICDD PDF-2 database (International Center for Diffraction Data). The crystallite size τ was calculated using Scherrer's equation [29]:

$$\tau = \frac{K\lambda}{\beta \cos\theta} \tag{1}$$

where K is a dimensionless shape factor (it was considered K = 0.9), λ is the X-ray wavelength (λ = 1.5406 Å for a Cu K_α source), β is the full width at half maximum FWHM and θ is the Bragg angle.

Thermogravimetry analysis and differential thermal analysis (DTA/TG STA409, Netzsch, Italy) were carried out in static atmospheric air, from room temperature to 1000 °C, with a heating rate of 5 °C/min.

Helium pycnometry (AccuPyc 1330, Micrometrics, Italy) was performed on printed structures as well as on finely ground powders; the open, closed and total porosity of the samples were also evaluated.

Uniaxial compression tests were performed on the printed lattices using a universal testing machine (1121 UTM, Instron, Italy), equipped

with a 10 KN load cell; the crosshead speed was set at 1 mm/min. At least 5 samples per composition were tested; resulting values were indicated as mean ± standard deviation.

Shrinkage values were evaluated using a digital caliper taking at least 2 measurements per each side, per sample.

The development of the geopolymeric network upon curing was further assessed by ATR - FTIR spectroscopy (6200 FTIR spectrometer equipped with ATR Pro One diamond prism, Jasco Inc., Italy) in the 1500–400 cm^{-1} range. Absorbance spectra were determined for fine powders from printed GP structures after each curing condition; the data are reported in the Supplementary Information.

3. Results and discussion

3.1. Rheological characterization of the inks

The addition of a filler has the main goal of increasing the printability of an ink, i.e. its viscosity and yield strength, without affecting the H$_2$O/Al$_2$O$_3$ molar ratio of the geopolymer. In fact, while a lower water amount may be beneficial for the final mechanical properties of the component, there are practical limitations related to the solubility of the alkali hydroxides and silicates and to the effective mixing with the metakaolin. Moreover, a higher amount of water contributes to the synthesis of geopolymer with higher specific surface area (SSA) and meso-porosity, desirable qualities for applications as filters, catalyst carriers, and so on.

The addition of a filler influences also the mechanical properties of the final part: on one hand, fillers with high strength contribute to the strength of the final part; on the other hand, hindered shrinkage and thermal expansion coefficient (CTE) mismatch between matrix and filler can result in cracks that compromise such strength.

Based on these considerations, two different kinds of fillers were selected:

- siliceous sand (commercially available, possessing high mechanical properties);

- geopolymer powder (same composition as the matrix, i.e. similar SSA and CTE).

The rheological characteristics of the resulting GPS and GPP inks are reported in Fig. 1, together with those for a GP ink without any fillers [16].

As shown in Fig. 1a, GPS and GPP retained the Bingham pseudoplastic behavior displayed by the pure geopolymer ink GP, but the flow curves shifted to higher stresses (and viscosities) for the same shear rate. The effect of the geopolymeric filler is more pronounced compared to that of the siliceous sand; this can be related to the smaller dimensions of the ground geopolymer particles, as well as to their higher chemical affinity with the developing matrix. In fact, residual Al–OH and Si–OH groups are usually present in geopolymers after drying; in this case, O–H bending and stretching peaks were detected in the FTIR spectra of pure geopolymer for all curing conditions (see Fig. S2) [30]. The surface of the particles may be subject to a secondary condensation with the developing matrix, resulting in hindered flow. Similar secondary condensation has been observed between geopolymer particles processed by warm pressing [31].

The same trend was detected when carrying out the dynamic strain sweep test (Fig. 1b). At low strains, G′ and G″ showed a plateau (corresponding to the linear viscoelastic region). Their subsequent drop at intermediate strains was interpreted as the yield point, as it represented the onset of non-linearity; it corresponded to an inflection in the shear stress – strain curves. The region is highlighted in the graph and the values are reported in Table 1 as mean value ± standard deviation in the inflection

Table 1
Values of τ_y, G′$_{max}$ and G′$_S$ for the three inks from the dynamic strain sweep test.

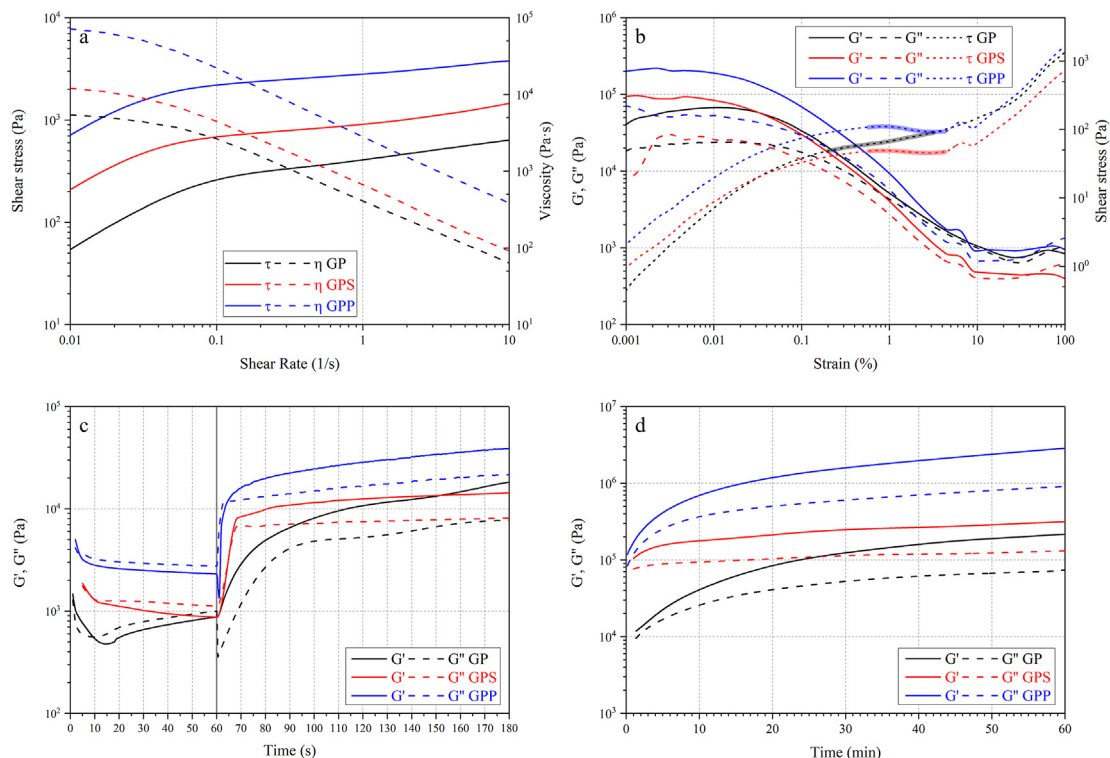|	GP	GPS	GPP
τ_y *(Pa)*	66 ± 13	47 ± 1	101 ± 8
G′$_{max}$ (Pa)	67.2 10^3	93.4 10^3	234.9 10^3
G′$_S$ (Pa)	76	86	79

Fig. 1. Rheological characterization of the three inks. a) flow curves; b) dynamic strain sweeps; c) moduli recovery and d) working time tests.

region. The G' value in the elastic region provides information about the ink stiffness once deposited. Smay et al. [32] demonstrated that in order to have a minimal deflection (<5% of the filament diameter) the following relation must be satisfied:

$$G^{'} \geq G_S^{'} = 0.35\gamma \left(\frac{L}{D}\right)^4 D \tag{2}$$

where γ is the specific weight of the ink, L is the span gap and D the filament diameter. γ can be derived from the ink density, which is calculated using the rule of mixture from the theoretical density of the individual raw materials: it was 1.73 g/cm^3 for the GP ink. As GPP ink contained 20 vol% of ground geopolymer filler with a true density of 1.99 g/cm^3 (measured by helium pycnometry), its density was slightly higher (1.79 g/cm^3). GPS ink possessed the highest density (1.95 g/cm^3) due to the presence of sand (true density of 2.73 g/cm^3, measured by helium pycnometry). L was set at 1.6 mm and D was set at 0.8 mm. Resulting values are reported in Table 1 and compared with the maximum value measured for G' in the linear viscoelastic region.

Results confirm that the geopolymer ink without any fillers is perfectly suitable for the fabrication of the suspended struts present in the lattices ($G^{'}_{max} \gg G^{'}_S$); however, the inks containing fillers exhibited higher $G^{'}_{max}$ values compared to their filler-free counterpart. The difference is much more significant for GPP ink, in agreement with what previously observed. The yield stress is lower for GPS ink than for the pure GP ink: the presence of sand particles might inhibit the gel network formation, resulting in weaker bonds that could be broken at lower stresses. GPP ink, on the contrary, showed the highest yield stress, in accordance with the higher affinity of powder and matrix. A higher yield stress is a particularly beneficial feature, as it allows for the manufacturing of larger samples with a greater number of layers that will not collapse under their own weight.

Recovery tests conducted in oscillation mode confirmed the suitability of the inks for DIW (Fig. 1c). As expected from the strain sweep tests, the plateau values of G' and G" are similar for the GP and GPS inks, and higher for the GPP ink. Their recovery in the second stage of the test was quicker for the inks containing fillers: while the GP ink required ~45 s for an increase by one order of magnitude of its G' modulus, the GPS ink needed only ~10 s. The GPP ink required ~30 s for the same relative increase, but only ~3 s to reach values similar to the GPS and GPP plateau. The presence of particles provided the inks with higher rigidity and viscosity; therefore, their deformation is limited and, as a result, their structural recovery is faster. The fast increase to high values of G' limits further deformation (slumping due to gravity) of the deposited filaments.

Finally, the working time of the three inks was compared (Fig. 1d). All inks showed an initially fast increase of G' and G", followed by a much slower ramp. Their slope was the highest for pure GP ink, corresponding to a printing window of ~1.5 h. Typically, filler-containing inks could be printed for longer times (up to 3 h), allowing to fabricate bigger components. It appears that the fillers acted as a retardant, possibly due to steric shielding of the activated moieties in the ink; the effect is more pronounced for the GPS ink, showing the lowest slope; this is in accordance with what observed from the dynamic strain sweep test. The possibility of extending the working window, which is the time in which the viscosity does not significantly change, is particularly relevant considering that a geopolymeric ink is a reactive medium and therefore its rheology is bound to change with time, requiring a continuous
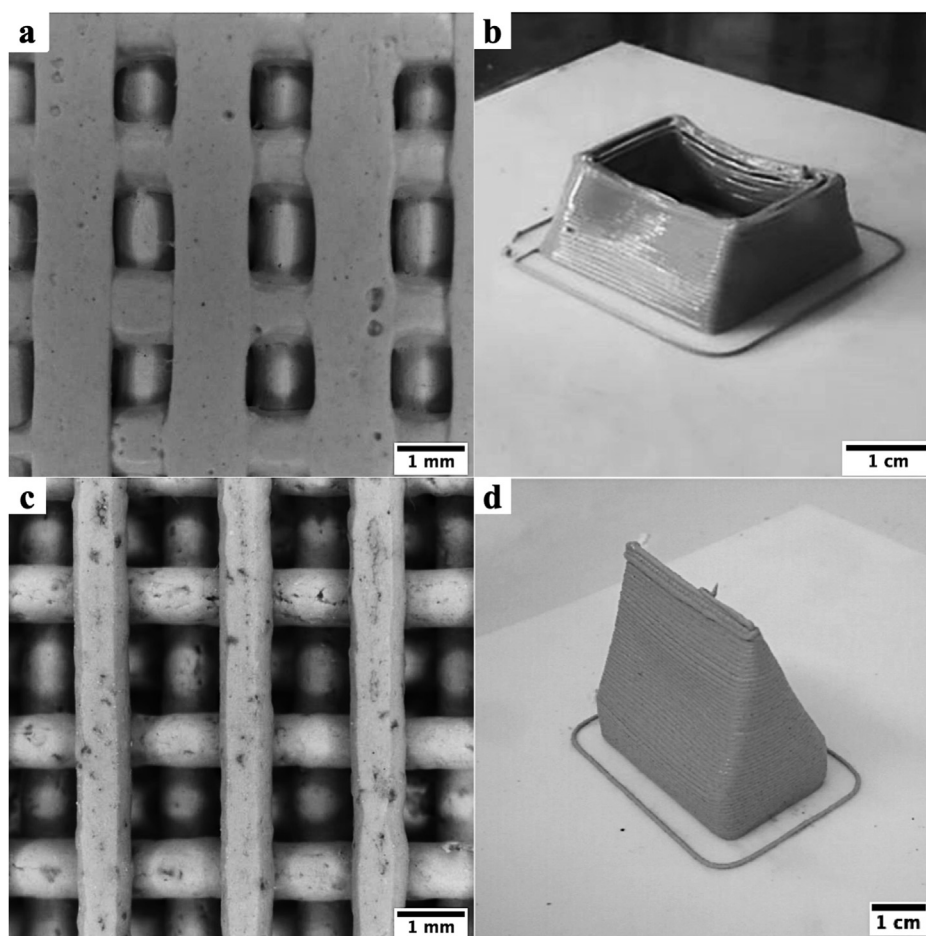

Fig. 2. Examples of lattices with overhangs and of a tall structure (slope angle = 20° with respect to the normal) printed with GP (a, b) and GPS (c, d) inks. a) and c): bottom layer of the scaffold.

adjustment of the printing parameters, which would not be simple to implement.

Fig. 2 provides a comparison of lattices and tall parts printed with the GP and GPS inks (with up to 40 vol% sand), confirming the ability of inks containing fillers to produce larger structures and higher overhangs with much lower deformation caused by sagging. With a designed height of 7.2 mm, GP lattices after printing were only 6.80 ± 0.15 mm tall, while GPS and GPP ones were 7.14 ± 0.15 mm and 7.19 ± 0.15 mm tall, respectively. Moreover, the addition of an inert filler eliminated the deformation of the first layer deposited on the substrate when printing, and reduced sagging of unsupported areas in the struts as well as the shrinkage upon drying.

3.2. Effect of the fillers upon curing

The geopolymerization reaction can occur at room temperature, but depending on the composition it can take up to a month to be completed [1]; over time, a compact 3D network is formed, which results in higher mechanical properties of the material. The reaction consists of many steps; although most of them are exothermic, the induction period, which governs the overall kinetics of the reaction, is endothermic in nature. Addition of heat reduces the induction period and expedites the reaction. Therefore, the reaction can be promoted by increasing the curing temperature [1,33].

The effect of different curing treatments on lattices printed with the three inks was evaluated by uniaxial compressive tests on samples cured at room temperature (~20 °C), 40 °C and 80 °C over a period of 1 day and 7 days. All samples showed a non-catastrophic failure upon fracture, which is typical for cellular structures [34]. Results are reported in Fig. 3.

The compressive strength of lattices produced with all three inks seemed to increase slightly for samples cured at higher temperatures and for longer time, in accordance with literature [35]. However, data were too dispersed to identify a significant difference between the treatments nor a specific trend. FT-IR spectra of the GP samples, collected after the different curing treatments, confirmed that they all reached a similar stage in the polycondensation reaction (see Fig. S2, supplementary information). The reaction may not be completed after 7 days; however, it can be assumed that all samples of the same composition would reach a similar compressive strength after the same curing treatment [35]. For this reason, further optimization was performed on samples cured at 80 °C for 1 day, which was considered the best compromise between mechanical performance and curing time.

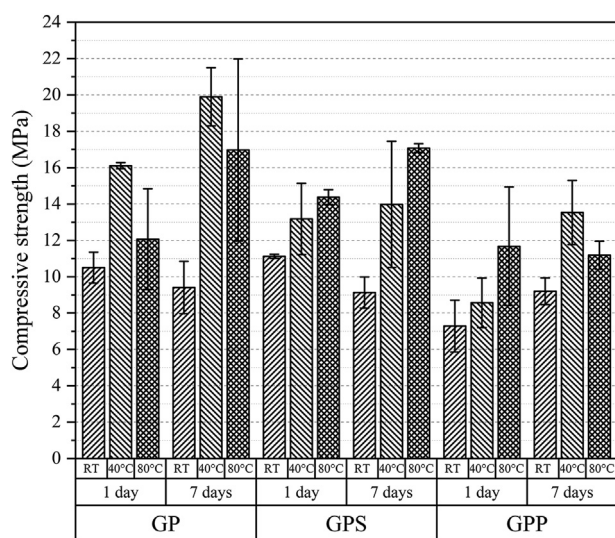The addition of a high strength particle filler (sand) did not improve the compressive strength of the printed GPS lattices significantly; the amount of filler may have been too low for an effective load distribution and for the activation of crack deflection mechanisms (as observed in cement mortars [36]).

In the case of GPP lattices, the geopolymer powder had the same properties as the matrix and their chemical affinity likely produced a strong interface; therefore, no strengthening mechanism could take place. The addition of this filler seemed even slightly detrimental, possibly due to the formation of an interrupted, weakened network.

3.3. Effect of different firing temperatures

Fig. 4 shows the results of the thermal analysis performed on the geopolymer matrix right after curing at 80 °C. An endothermic peak can be detected at approximately 110 °C, corresponding to the evaporation of physical water. An exothermic peak is evident at around 250 °C, corresponding to the polycondensation into siloxo bonds for the unreacted phase in the geopolymer powder [1]. At around 700 °C, another exothermic peak is observed, corresponding to the formation of a crystal phase (see below), followed by another small crystallization peak located at ~900 °C. The first peaks of the DTA curve, associated to the release of water species, resulted in the largest weight loss, which continued throughout the whole test up to 23 wt% at 1000 °C. The weight loss at high temperatures could be attributed to the reduction of the sodium amount within the material after the decomposition of the O–Na group [37].

The effect of different firing treatments on the geopolymer matrix was evaluated by X-ray diffractometry on samples treated at 80 °C (curing treatment), 300 °C, 500 °C, 700 °C and 1000 °C. Results are reported in Fig. 5. As expected, the geopolymer matrix consolidated forming a denser amorphous network; the detected peaks belong to quartz (Q; entry 96-900-9667; principal peaks at 20.9° and 26.6°), anatase (A; entry 96-900-9087; principal peaks at 25.3°) and muscovite (M; entry 96-101-1050; principal peak at 19.8°), which are present as impurities in the metakaolin raw material and do not participate in the geopolymerization reaction. The center of the amorphous halo shifted slightly to the left from about 28° after curing at 80 °C to about 24° after firing at 700 °C. This could be attributed to the formation of nanocrystalline domains of hydroxy-sodalite zeolite (Na_8 $[AlSiO_4]_6(OH)_2$) within the geopolymer amorphous network, in agreement with the DTA data, which would be too small to be detected with the XRD technique [38]. The geopolymer had a Si:Al = 1.9 ratio, whereas hydroxy-sodalite requires Si:Al = 1; therefore, a higher amount of silica would be expected in the remaining amorphous matrix, resulting in the shifting of the amorphous halo to lower angles [39]. Increasing the firing temperature to 1000 °C led to the formation of Nepheline (N; entry 96-900-1951), notwithstanding the
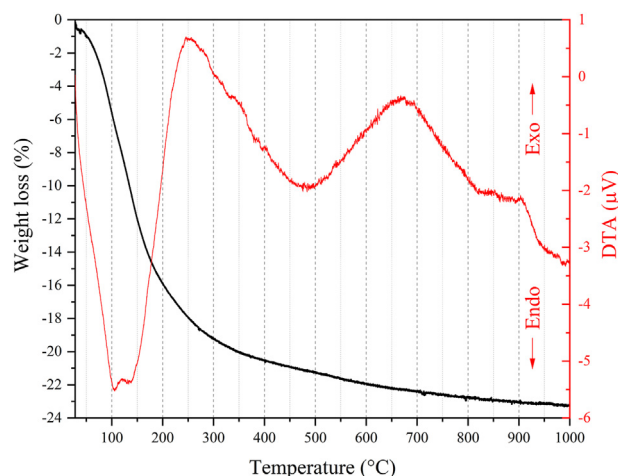

Fig. 3. Compressive strength of GP, GPS and GPP lattices after different curing treatments.

Fig. 4. DTA/TGA analysis of the geopolymer matrix.
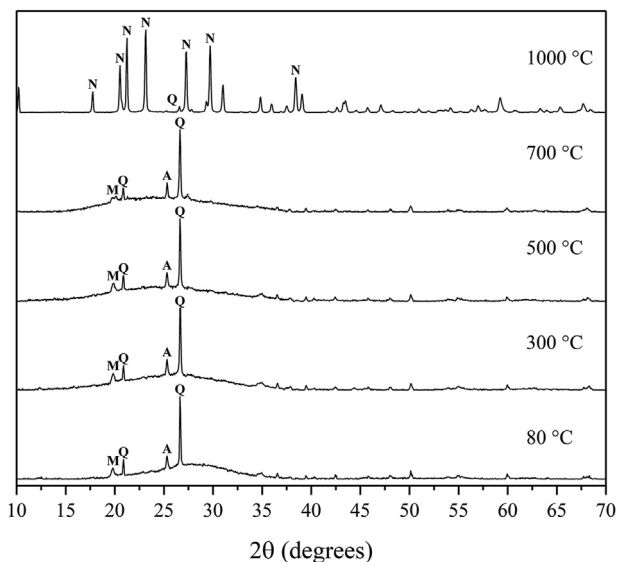
Fig. 5. XRD analysis of the geopolymer matrix (Q: quartz; A: anatase; M: muscovite; N: nepheline).

Table 2
Total porosity (%_vol) and volumetric shrinkage (%_vol) of the printed lattices after the firing treatments (samples cured at 80 °C for 1 day were used as reference).

		80 °C	300 °C	500 °C	700 °C	1000 °C
GP	Total porosity	51 ± 2%	54 ± 2%	59 ± 5%	60 ± 4%	65 ± 4%
	Volumetric shrinkage	reference	−20 ± 2%	−20 ± 2%	−30 ± 4%	−24 ± 8%
GPS	Total porosity	49 ± 2%	59 ± 2%	60 ± 3%	62 ± 3%	63 ± 4%
	Volumetric shrinkage	reference	−10 ± 1%	−14 ± 1%	−25 ± 2%	−23 ± 3%
GPP	Total porosity	50 ± 3%	61 ± 2%	63 ± 4%	62 ± 5%	67 ± 4%
	Volumetric shrinkage	reference	−17 ± 1%	−14 ± 1%	−17 ± 4%	−16 ± 4%

resilience to crystallization of the amorphous phase of a Na-geopolymer with a high Si/Al ratio [6]. The average crystallite size was 49.4 ± 1.3 nm, too small to be detected in the ESEM micrographs (see Fig. 8).

The different firing treatments affected the lattices' microstructure as well as their mechanical properties. Uniaxial compressive strength after each firing treatment on the GP, GPS and GPP printed lattices is reported in Fig. 6. Total porosity and volumetric shrinkage are reported in Table 2. Values for samples only cured at 80 °C for 1 day are reported as reference, i.e. their shrinkage value is set to a value of 0.

Pure GP lattices were the most affected by the thermal treatments: they showed a maximum compressive strength of 34 ± 3 MPa after firing at 300 °C, followed by a rapid decrease at higher temperatures reaching a minimum of 4.0 ± 0.6 MPa at 1000 °C. GPS, on the other hand, showed a consistent decrease in the compressive strength (~30%) already after firing at 300 °C, and a progressive decrease in the mechanical properties with increasing firing temperatures. Finally, GPP lattices were the least affected by the treatments: aside from data fluctuation, their compressive strength was ~10 MPa for all firing temperatures.

The different trends detected for the three compositions can be explained based on their microstructure (Fig. 7 and Fig. 8) and on the
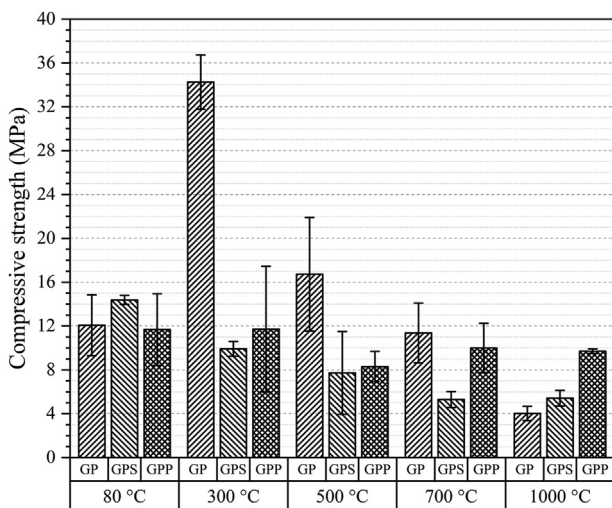
DTA/TGA analysis (Fig. 4). At 300 °C, water is completely removed from the structures through the polycondensation of bonding siloxo groups, producing a strong 3D network; the reaction is associated with volumetric shrinkage. GP and GPP lattices showed similar shrinkage and negligible cracking (see Fig. 7a and c), which was attributed to sample preparation and handling. GPS samples, on the other hand, experienced a lower shrinkage and were severely cracked (Fig. 7b). Upon heating, in fact, the sand filler slightly expanded and hindered the shrinkage of the matrix, generating tensions that originated the cracks. Such issue did not occur in GPP samples, as the filler and matrix behave in the same way. Therefore, sand provides for a cheap and effective filler for applications at room temperature, but it cannot be used for applications that require heating.

It is worth to observe that at high temperatures GPP performed better than its pure GP counterpart. The compressive strength of GPP lattices at 1000 °C was comparable to that at room temperature, whereas for GP lattices it was reduced to about 1/3 of its initial value. The higher solid content in the GPP inks likely resulted in the lower shrinkage measured for the GPP lattices, and therefore in lower crack-inducing stresses. GP and GPP inks had the same chemical composition, but their microstructure was slightly different, especially at high temperatures. ESEM micrographs at 1000 °C do not allow to detect nepheline crystals, but they rather show the effect of a viscous flow likely provided by the remaining amorphous silica-rich matrix. This was more pronounced in pure GP samples (Fig. 8a and b); GPP structures (Fig. 8c and d) seem less affected, possibly due to the presence of particle/matrix interfaces which hinder the viscous flow.

The designed porosity calculated from the CAD file, assuming dense, cylindrical struts, was 55.5 vol%. It corresponds to the open macro-channels produced by the layers build-up. After curing, all samples showed values slightly below the designed porosity. This can be attributed to a deviation from the model file caused by non-optimal process parameters, and resulting for example in filaments with larger diameter, as well as to some limited sagging where the filaments are not supported. Some pores were also detected within the struts, caused by air entrapped into the slurry while mixing. There was a high variability within the results; however, a general trend can be recognized in all samples, i.e. an increase of the total porosity with increasing firing temperature. This is particularly relevant when comparing samples cured at 80 °C and fired at 300 °C and can be linked to the evaporation of water and the completion of the polycondensation reaction, as well as the removal of the organic additive (PEG). This trend is in accordance with the weight loss detected with the TGA analysis (Fig. 4) and with the general decrease of compressive strength for the higher firing temperatures (Fig. 6). The presence of some cracks could also account for the increase in total porosity of the samples. Moreover, the formation of crystals with a higher density than the original matrix, as is the case for nepheline and the pure geopolymer, could also lead to the formation of distributed porosity, as it has been reported to occur in geopolymers [37,40] as well as in
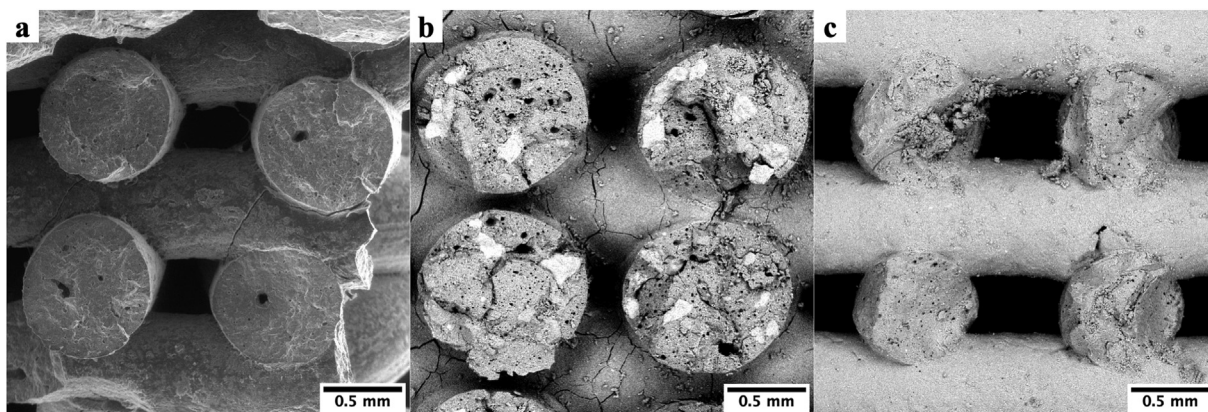

Fig. 6. Compressive strength values for GP, GPS and GPP lattices with different firing treatments.

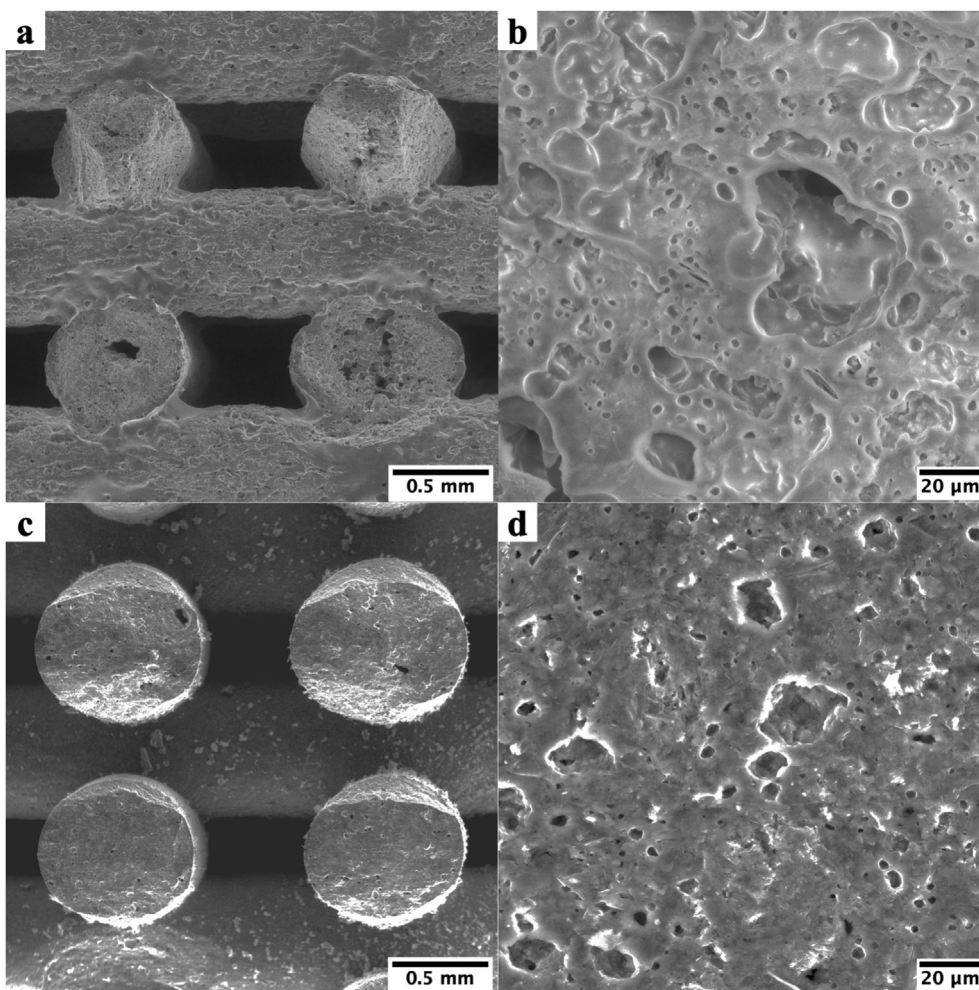**Fig. 7.** SEM micrographs of a) GP, b) GPS and c) GPP lattices after firing at 300 °C.

Fig. 8. SEM micrographs of a) GP and c) GPP lattices after firing at 1000 °C. b) and d) show higher magnifications of samples GP and GPP, respectively.

glass-ceramics [41,42].

4. Conclusions

The addition of a particulate filler to a pure geopolymer ink (GP), either sand (GPS) or ground geopolymer (GPP), enhanced its rheological properties. Ground geopolymer filler was the most effective, due to its smaller dimension and higher affinity with the matrix. In particular, the yield strength τ_Y and storage modulus G' were increased, the time required for the recovery of G' and G'' values once extruded was reduced and the working window was expanded.

The mechanical properties of lattices printed using inks containing fillers (GPS and GPP) did not increase significantly, possibly due to the relatively low amount of filler employed; in the case of GPP, the compressive strength was slightly lower than that of pure GP lattices. Increasing curing temperature and time (up to 80 °C for 7 days) did not seem to affect the compressive strength significantly.

Heating lattices at 300 °C caused an increase in strength for GP

samples up to 34 ± 3 MPa, while GPS samples showed a decrease in strength due to the formation of cracks in the geopolymer matrix, caused by the different thermal behavior of filler and matrix. With increasing firing temperature, the porosity of all the lattices increased, leading to a decrease in their compressive strength. GPP samples were the least affected by the thermal treatments and maintained a compressive strength of 9.7 ± 0.2 MPa after firing at 1000 °C with a total porosity of 67 ± 4 vol%.

We can therefore infer that the addition of particle fillers resulted in improved rheological properties and better printability of the geopolymer inks. Sand provided for a cheap and effective reinforcement at room temperature, but it cannot be used for applications that require heating. Ground geopolymer powder, on the other hand, resulted in less thermal damage at high temperature, enabling a better retention of the shape of the lattices upon heating.

The geopolymer lattices developed in this work, depending on the composition of the ink used to manufacture them, could be used as filters for water or gas purification or as catalyst supports working at medium to high temperature. Further investigations will focus on the validation of additional geopolymer compositions and on DIW of scaffolds based on geopolymer composites reinforced using short fibers (e.g. carbon or AR glass), potentially providing enhanced flexural strength.

Acknowledgments

Appendix A. Supplementary data

Supplementary data to this article can be found online at https ://doi.org/10.1016/j.oceram.2021.100134.

References

[1] J. Davidovits, Geopolymer Chemistry and Applications, fifth ed., Institut Geopolymere, 2020.

[2] J.S.J. Van Deventer, J.L. Provis, P. Duxson, Technical and commercial progress in the adoption of geopolymer cement, Miner. Eng. 29 (2012) 89–104, https://doi.org/10.1016/j.mineng.2011.09.009.

[3] A. Hassan, M. Arif, M. Shariq, Use of geopolymer concrete for a cleaner and sustainable environment – a review of mechanical properties and microstructure, J. Clean. Prod. 223 (2019) 704–728, https://doi.org/10.1016/j.jclepro.2019.03.051.

[4] G. Fahim Huseien, J. Mirza, M. Ismail, S.K. Ghoshal, A. Abdulameer Hussein, Geopolymer mortars as sustainable repair material: a comprehensive review, Renew. Sustain. Energy Rev. 80 (2017) 54–74, https://doi.org/10.1016/j.rser.2017.05.076.

[5] C. Bai, P. Colombo, Processing, properties and applications of highly porous geopolymers: a review, Ceram. Int. 44 (2018) 16103–16118, https://doi.org/10.1016/j.ceramint.2018.05.219.

[6] P. Duxson, G.C. Lukey, J.S.J.J. Van Deventer, Evolution of gel structure during thermal processing of Na-geopolymer gels, Langmuir 22 (2006) 8750–8757, https://doi.org/10.1021/la0604026.

[7] P. He, D. Jia, S. Wang, Microstructure and integrity of leucite ceramic derived from potassium-based geopolymer precursor, J. Eur. Ceram. Soc. 33 (2013) 689–698, https://doi.org/10.1016/j.jeurceramsoc.2012.10.019.

[8] P. He, R. Wang, S. Fu, M. Wang, D. Cai, G. Ma, M. Wang, J. Yuan, Z. Yang, X. Duan, Y. Wang, D. Jia, Y. Zhou, Safe trapping of cesium into doping-enhanced pollucite structure by geopolymer precursor technique, J. Hazard Mater. 367 (2019) 577–588, https://doi.org/10.1016/j.jhazmat.2019.01.013.

[9] H. Wang, H. Li, Y. Wang, F. Yan, Preparation of macroporous ceramic from metakaolinite-based geopolymer by calcination, Ceram. Int. 41 (2015) 11177–11183, https://doi.org/10.1016/j.ceramint.2015.05.067.

[10] A. Rincón Romero, H. Elsayed, E. Bernardo, Highly porous mullite ceramics from engineered alkali activated suspensions, J. Am. Ceram. Soc. 101 (2018) 1036–1041, https://doi.org/10.1111/jace.15327.

[11] C. Bagci, Q. Yang, W.M. Kriven, Formation of α/β-Si3N4 nanoparticles by carbothermal reduction and nitridation of geopolymers, J. Am. Ceram. Soc. 102 (2019) 6542–6551, https://doi.org/10.1111/jace.16545.

[12] C. Bagci, G.P. Kutyla, K.C. Seymour, W.M. Kriven, Synthesis and characterization of silicon carbide powders converted from metakaolin-based geopolymer, J. Am. Ceram. Soc. 99 (2016) 2521–2530, https://doi.org/10.1111/jace.14254.

[13] K. Sakkas, P. Nomikos, A. Sofianos, D. Panias, Sodium-based fire resistant geopolymer for passive fire protection, Fire Mater. 39 (2015) 259–270, https://doi.org/10.1002/fam.2244.

[14] M. Xia, J.G. Sanjayan, J.G. Sanjayan, Method of formulating geopolymer for 3D printing for construction applications, Mater. Des. 110 (2016) 382–390, https://doi.org/10.1016/j.matdes.2016.07.136.

[15] M. Xia, J.G. Sanjayan, Methods of enhancing strength of geopolymer produced from powder-based 3D printing process, Mater. Lett. 227 (2018) 281–283, https://doi.org/10.1016/j.matlet.2018.05.100.

[16] G. Franchin, P. Scanferla, L. Zeffiro, H. Elsayed, A. Baliello, G. Giacomello, M. Pasetto, P. Colombo, Direct ink writing of geopolymeric inks, J. Eur. Ceram. Soc. 37 (2017), https://doi.org/10.1016/j.jeurceramsoc.2017.01.030.

[17] J. Zhong, G.X. Zhou, P.G. He, Z.H. Yang, D.C. Jia, 3D printing strong and conductive geo-polymer nanocomposite structures modified by graphene oxide, Carbon N. Y. 117 (2017) 421–426, https://doi.org/10.1016/j.carbon.2017.02.102.

[18] B. Panda, S.C. Paul, L.J. Hui, Y. Wei, D. Tay, M. Jen, Y.W.D. Tay, M.J. Tan, Y. Wei, D. Tay, M. Jen, Y.W.D. Tay, M.J. Tan, Additive manufacturing of geopolymer for sustainable built environment, J. Clean. Prod. 167 (2018) 281–288, https://doi.org/10.1016/j.jclepro.2017.08.165.

[19] B. Panda, C. Unluer, M.J. Tan, Extrusion and rheology characterization of geopolymer nanocomposites used in 3D printing, Compos. B Eng. 176 (2019), https://doi.org/10.1016/j.compositesb.2019.107290.

[20] J.H. Lim, B. Panda, Q.C. Pham, Improving flexural characteristics of 3D printed geopolymer composites with in-process steel cable reinforcement, Construct. Build. Mater. 178 (2018) 32–41, https://doi.org/10.1016/j.conbuildmat.2018.05.010.

[21] S. Muthukrishnan, W. Kua Harn, N. Yu Ling, J.K.H. Chung, Fresh Properties of Cementitious Materials Containing Rice Husk Ash for Construction 3D Printing, 2020, https://doi.org/10.1061/(ASCE)MT.1943-5533.0003230.

[22] M.F. Alnahhal, T. Kim, A. Hajimohammadi, Distinctive rheological and temporal viscoelastic behaviour of alkali-activated fly ash/slag pastes : a comparative study with cement paste, Cement Concr. Res. 144 (2021) 106441, https://doi.org/10.1016/j.cemconres.2021.106441.

[23] S. Muthukrishnan, S. Ramakrishnan, J. Sanjayan, Effect of alkali reactions on the rheology of one-part 3D printable geopolymer concrete, Cement Concr. Compos. 116 (2021), https://doi.org/10.1016/j.cemconcomp.2020.103899.

[24] G. Franchin, J. Pesonen, T. Luukkonen, C. Bai, P. Scanferla, R. Botti, S. Carturan, M. Innocentini, P. Colombo, Removal of ammonium from wastewater with geopolymer sorbents fabricated via additive manufacturing, Mater. Des. 195 (2020), 109006, https://doi.org/10.1016/j.matdes.2020.109006.

[25] M.D.M. Innocentini, R.F. Botti, P.M. Bassi, C.F.P.R. Paschoalato, D.L. Flumignan, G. Franchin, P. Colombo, Lattice-shaped geopolymer catalyst for biodiesel synthesis fabricated by additive manufacturing, Ceram. Int. 45 (2019) 1443–1446, https://doi.org/10.1016/j.ceramint.2018.09.239.

[26] P. Avila, M. Montes, E.E. Miró, Monolithic reactors for environmental applications A review on preparation technologies, Chem. Eng. J. 109 (2005) 11–36, https://doi.org/10.1016/j.cej.2005.02.025.

[27] W.M. Carty, P.W. Lednor, Monolithic ceramics and heterogeneous catalysts: honeycombs and foams, Curr. Opin. Solid State Mater. Sci. 1 (1996) 88–95.

[28] O. Al-Ketan, M. Pelanconi, A. Ortona, R.K. Abu Al-Rub, Additive manufacturing of architected catalytic ceramic substrates based on triply periodic minimal surfaces, J. Am. Ceram. Soc. 102 (2019) 6176–6193, https://doi.org/10.1111/jace.16474.

[29] A.L. Patterson, The scherrer formula for X-ray particle size determination, Phys. Rev. 56 (1939) 978–982, https://doi.org/10.1103/PhysRev.56.978.

[30] M.F. Zawrah, S.E. Abo Sawan, R.M. Khattab, A.A. Abdel-Shafi, Effect of nano sand on the properties of metakaolin-based geopolymer: study on its low rate sintering, Construct. Build. Mater. 246 (2020), https://doi.org/10.1016/j.conbuildmat.2020.118486.

[31] H. Takeda, S. Hashimoto, H. Matsui, S. Honda, Y. Iwamoto, Rapid fabrication of highly dense geopolymers using a warm press method and their ability to absorb neutron irradiation, Construct. Build. Mater. 50 (2014) 82–86, https://doi.org/10.1016/j.conbuildmat.2013.09.014.

[32] J.E. Smay, J. Cesarano, J.A. Lewis, Colloidal inks for directed assembly of 3-D periodic structures, Langumuir 18 (2002) 5429–5437, https://doi.org/10.1021/la0257135.

[33] M. Rosnita, A.R. Rafiza, M.A.B.A. Mohd, A review on heat released in early geopolymerization by calorimetric study. Mater. Sci. Forum, Trans Tech Publications Ltd, 2019, pp. 236–240. https://doi.org/10.4028/www.scientific.net/MSF.967.236.

[34] M. Scheffler, P. Colombo, Cellular Ceramics Structure, Manufacturing, Properties and Applications, 2005.

[35] P. Rovnaník, Effect of curing temperature on the development of hard structure of metakaolin-based geopolymer, Construct. Build. Mater. 24 (2010) 1176–1183, https://doi.org/10.1016/j.conbuildmat.2009.12.023.

[36] J. Bu, Z. Tian, S. Zheng, Z. Tang, Effect of sand content on strength and pore structure of cement mortar, J. Wuhan Univ. Technol.-Materials Sci. Ed. 32 (2017) 382–390, https://doi.org/10.1007/s11595-017-1607-9.

[37] L.M. Kljajević, S.S. Nenadović, M.T. Nenadović, N.K. Bundaleski, B. Todorović, V.B. Pavlović, Z.L. Rakočević, Structural and chemical properties of thermally treated geopolymer samples, Ceram. Int. 43 (2017) 6700–6708, https://doi.org/10.1016/j.ceramint.2017.02.066.

[38] J.L. Provis, G.C. Lukey, J.S.J. Van Deventer, Do geopolymers actually contain nanocrystalline zeolites? a reexamination of existing results, Chem. Mater. 17 (2005) 3075–3085, https://doi.org/10.1021/cm050230i.

[39] E.M. An, Y.H. Cho, C.M. Chon, D.G. Lee, S. Lee, Synthesizing and assessing fire-resistant geopolymer from rejected fly ash, J. Korean Ceram. Soc. 52 (2015) 253–263, https://doi.org/10.4191/kcers.2015.52.4.253.

[40] Y.M. Liew, C.Y. Heah, L. yuan Li, N.A. Jaya, M.M.A.B. Abdullah, S.J. Tan, K. Hussin, Formation of one-part-mixing geopolymers and geopolymer ceramics from geopolymer powder, Construct. Build. Mater. 156 (2017) 9–18, https://doi.org/10.1016/j.conbuildmat.2017.08.110.

[41] A. Karamanov, M. Pelino, Induced crystallization porosity and properties of sintereds diopside and wollastonite glass-ceramics, J. Eur. Ceram. Soc. 28 (2008) 555–562, https://doi.org/10.1016/j.jeurceramsoc.2007.08.001.

[42] E. Bernardo, R. Castellan, S. Hreglich, Sintered glass-ceramics from mixtures of wastes, Ceram. Int. 33 (2007) 27–33, https://doi.org/10.1016/j.ceramint.2005.07.012.